Terra Antartica
2007, **14**(1), 69-84

TERRA ANTARTICA
AN ANTARCTIC EARTH SCIENCE JOURNAL

Ultramafic Rocks in High-Strain Zones of the Southern Mawson Escarpment, Prince Charles Mountains (East Antarctica): Evidence for Major Crustal Shear Zones of the Palaeoarchaean Age?

E.V. Mikhalsky[1]*, F. Henjes-Kunst[2] & N.W. Roland[2]

[1]VNIIOkeangeologia, Angliisky ave. 1, St Petersburg 190121 - Russia
[2]Bundesanstalt für Geowissenschaften und Rohstoffe, Stilleweg 2, Hannover 30655 - Germany
**Corresponding author* (emikhalsky@mail.ru)

Received 7 May 2007; accepted in revised form 5 October 2007

Abstract - In the southern Mawson Escarpment, southern Prince Charles Mountains (Antarctica), lenses and blocks of compositionally highly diverse ultramafic and relatively rare mafic rocks are mostly confined to generally east–west trending high-strain shear zones. These rocks consist of amphibole (actinolite, tremolite, anthophyllite or, rarely hornblende), sporadically orthopyroxene, olivine and rarely clinopyroxene. Secondary talc, serpentine, epidote, phlogopite, carbonate, chlorite, and titanite are developed sporadically. Less sheared rocks include amphibole orthopyroxenite and amphibole dunite. The geochemical features of the ultramafic rocks point to a strong influence of accumulation processes. Sm–Nd whole rock and mineral separate data point to an origin from a highly heterogeneous Archaean mantle which comprises at least a highly depleted and an enriched component. The latter may represent a metasomatically reworked depleted reservoir. The LILE enrichment probably occurred already in the early Archaean. U–Pb zircon SHRIMP dating of zircon from a syn-tectonic leucocratic quartz-feldspar vein associated with the ultramafics in a high-strain shear zone yields ages of 2539 ± 61 Ma (lower intercept) and 3333 ± 60 Ma (upper intercept). The *ca.* 3.3 Ga date is interpreted as a close estimate of the age of syn-tectonic vein formation and thus also the formation of the high-strain shear zone while the *ca.* 2.5 Ga date probably reflects a (tectono-)thermal overprint. The occurrence of lenses and blocks of ultramafic and subordinate mafic rocks of highly variable lithological, geochemical and Sm-Nd isotope composition in high-strain shear zones of the southern Mawson Escarpment is interpreted as a tectonic melange indicative of major deep-reaching crustal shear processes in Paleoarchaean times.

INTRODUCTION

Mafic and ultramafic rocks are geologically significant constituents in the southern Prince Charles Mountains (sPCM; Fig. 1 a, b). Previous workers (*c.f.*, Mikhalsky et al., 2001 and references therein) mainly investigated mafic to ultramafic rocks found as dykes in the southern part of the sPCM (southern Mawson Escarpment, Mts. Rymill, Stinear and Ruker). Blocks and lenses of ultramafic rocks as reported from the Mawson Escarpment, Mts Ruker and McCauley and Lawrence Hills in the southern PCM and also from the Radok Lake area and the Nilsson Rocks in the northern Prince Charles Mountains (Fig. 1; Mikhalsky et al., 2001 and references therein; Corvino & Henjes-Kunst, 2007; Mikhalsky et al. 2007) have not been studied in detail. Both types of occurrences of ultramafic to mafic rocks are especially abundant in the southern Mawson Escarpment which constitutes the eastern part of the sPCM (Fig. 1 b). The sPCM are mainly built up by the Archaean to Neoproterozoic Ruker Province (Phillips et al., 2006), termed Ruker Terrane by other authors (Tingey, 1991, Kamenev, 1993, Mikhalsky et al., 2006a) (Fig. 1). In this area, prominent magmatic and tectonothermal events were dated at *ca.* 3370–3390 Ma, 3180–3160 Ma and *ca.* 2790–2770 Ma (Boger et al., 2006, Mikhalsky et al., 2006b). So far, a *ca.* 2650 Ma age for a post-tectonic pegmatite puts the lower age limit for tectonic activities in the southern Mawson Escarpment (Boger et al., 2006).

The southern Mawson Escarpment is mostly built up by medium-grade metamorphic rocks: hornblende–biotite orthogneisses, granite-gneisses and plagiogneisses (the Mawson Orthogneiss) and metasedimentary rocks (pelitic and calcareous metasediments and quartzites etc. of the Menzies Series) with a few relics of granulite facies assemblages. The central and northern Mawson Escarpment was distinguished as a separate Palaeoproterozoic Lambert Terrane by Mikhalsky et al. (2006a). A prominent crustal formation episode in this terrane was dated at *ca.* 2.5 – 2.4 Ga (Mikhalsky et al. 2006a; Corvino & Henjes-Kunst 2007 and references therein).

In this paper we present geological, geochemical and isotopic data on ultramafic and spatially associated mafic rocks occurring as blocks and lenses mainly within high-strain shear zones in the southern Mawson Escarpment. Sampling was carried out during the Prince Charles Mountains Expedition of Germany and Australia (PCMEGA) in 2002/2003. The aim of this study is to reveal the compositional features of the

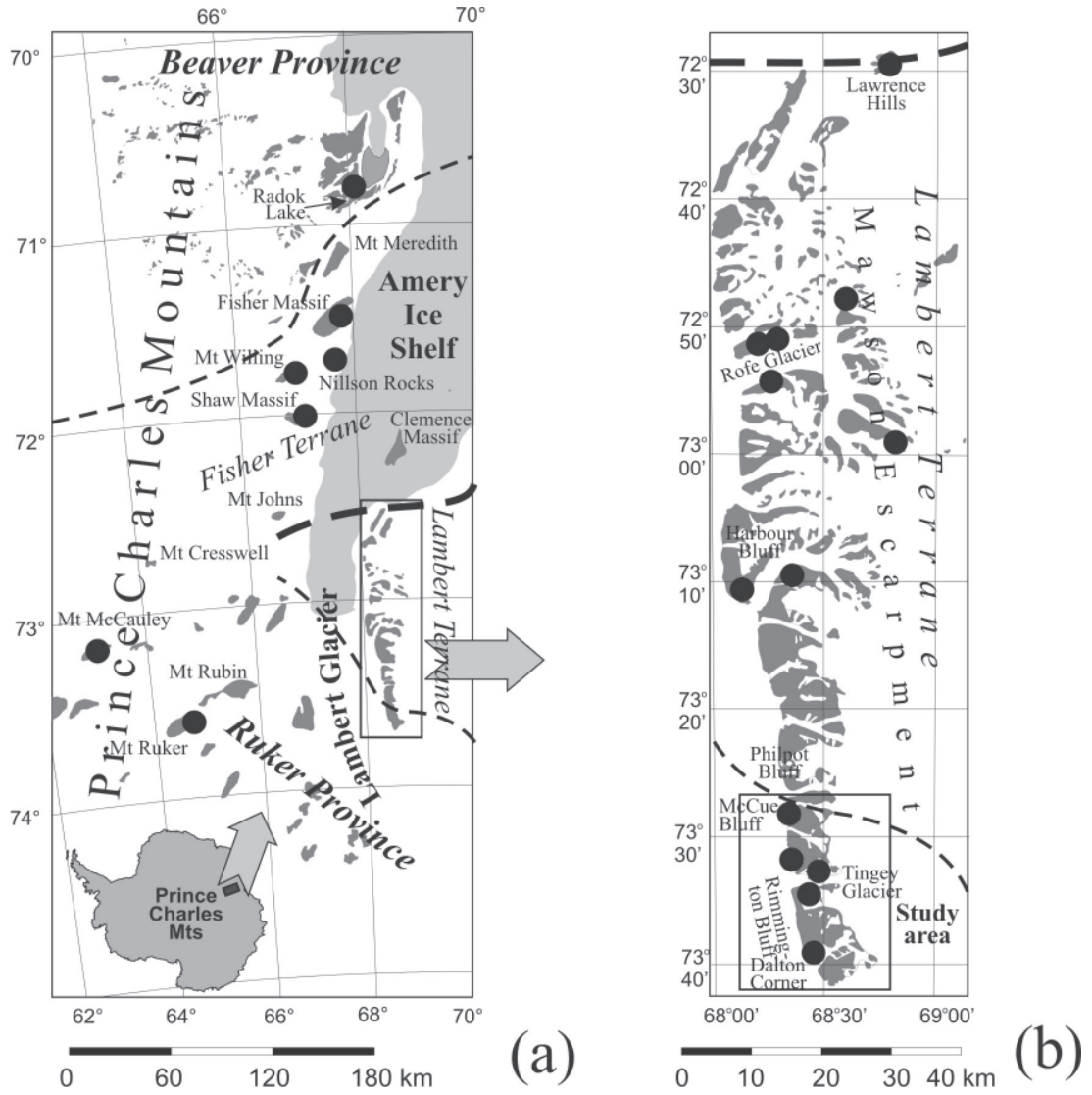

Fig. 1 - a) Locality map, also showing known occurrences of ultramafic rocks in the Prince Charles Mountains (thick dot). Boundaries of major tectonometamorphic provinces and terranes are marked by dashed lines. b) Rock outcrop area and coordinates in the Mawson Escarpment from the 1:200000 topographic map (Hydrometeoizdat, Moscow, 1978).

ultramafic to subordinate mafic rocks, to put some preliminary constraints on their age and origin by the means of geochemical and isotopic data, and to speculate about the geological significance of the association of compositionally different ultramafic to mafic rocks in high-strain shear zones of the southern Mawson Escarpment.

RESULTS

ANALYTICAL METHODS

Microprobe (EMP) investigation, major and trace element chemistry, and Sm-Nd isotope analysis were carried out in laboratories of Bundesanstalt für Geowissenschaften und Rohstoffe (BGR), Hannover, Germany. Concentrations of selected trace elements (REE, Hf, Nb, Ta, U, Th, Pb) were determined by ICP-MS analysis by Activation Laboratories Ltd. (Actlabs), Ancaster, Canada according to code 4B2 Research using the sample powders prepared at the BGR. SHRIMP dating of zircons was done at the Isotopic Centre (VSEGEI, St Petersburg, Russia).

For major and trace element chemistry and Sm-Nd isotope analysis, whole-rock powders were prepared using steel jaw crushers and an agate mortar. About 1-2 kg of sample material free of weathering crusts was used. Concentrations of major to minor elements were determined by X-Ray Fluorescence Spectrometry (XRF) on lithium borate glass fusion disks using automated PANalytical Axios and a PW 2400 spectrometers. EMP analysis was carried out using a Cameca SX100 electron microprobe with 15 kV acceleration voltage and 20 nA sample current. Natural minerals were used as standards: kaersutite (Si, Al, Mg, Ca, Ti), albite (Na), biotite (K), almandine (Fe), rhodonite (Mn) and chromite (Cr).

Sm-Nd isotope data were obtained using a ThermoFinnigan TRITON massspectrometer equipped with nine Faraday Cups. Element concentrations were determined by isotope-dilution techniques. Sample powders were decomposed with HF-HNO_3 in Teflon vessels after addition of the isotopic spikes

at temperatures close to 190 °C in the Picotrace™ pressure-digestion system DAS™. The lanthanides were separated on cation-exchange columns. Sm and Nd were isolated from each other and adjacent lanthanides in separate columns using HDEHP-coated Teflon powder (Cerrai & Testa 1963). Element fractions were loaded on Re filaments and run on a double-filament assembly in static mode. Isotopic ratios were normalized to $^{146}Nd/^{144}Nd = 0.7219$ for Nd. Procedural blanks are less than 0.1 % of the relevant sample concentration and are therefore negligible. A Nd element standard (Merck™) run routinely in the course of the sample measurements yielded $^{143}Nd/^{144}Nd = 0.512395$ (1SD = 0.000007; n = 4), which corresponds to $^{143}Nd/^{144}Nd = 0.511845$ for the LaJolla Nd standard (cross-calibrated at the BGR). Uncertainties at the 95 % confidence level are 0.005 % for $^{143}Nd/^{144}Nd$ and 1 % for $^{147}Sm/^{144}Nd$. Calculation of the Sm-Nd model parameters $\varepsilon_{Nd}(0)$ and $\varepsilon_{Nd}(t)$ (notation according to DePaolo 1988) is based on $^{143}Nd/^{144}Nd = 0.512638$ and $^{147}Sm/^{144}Nd = 0.1967$ for a CHUR reference ('chondritic uniform reservoir', Jacobsen & Wasserburg 1980). Single-stage depleted-mantle and CHUR model ages (T_{DM} and T_{CHUR}, respectively) were calculated according to DePaolo (1988) assuming $^{143}Nd/^{144}Nd = 0.513151$ and $^{147}Sm/^{144}Nd = 0.2136$ for the present-day depleted-mantle reservoir.

SHRIMP analysis was carried out using a SHRIMP-II Ionmicroprobe. Zircon grains were hand-picked and mounted in epoxy resin together with the TEMORA (Middledale Gabbroic Diorite, New South Wales, Australia) and 91500 (Geostandard zircon) reference zircons. The grains were sectioned approximately in half and polished. Reflected and transmitted light microphotographs and cathodoluminescence (CL) images were prepared for all zircons. The CL images were used to decipher the internal structures of the sectioned grains and to target specific areas within these zircons. Each SHRIMP U-Pb analysis consists of five scans through the mass range. Diameter of spot was about 18 µm, primary beam intensity was about 4 nA. The data have been reduced in a manner similar to that described by Williams (1998, and references therein), using the SQUID Excel Macro of Ludwig (2000). The Pb/U ratios have been normalized relative to a value of 0.0668 for the $^{206}Pb/^{238}U$ ratio of the TEMORA reference zircons, equivalent to an age of 416.75 Ma (Black and Kamo, 2003). Uncertainties given for individual analyses (ratios and ages) are at the 1σ level. The uncertainties in calculated concordia ages, however, are reported at the 2σ level. The Wetherill (1956) concordia plot has been prepared using ISOPLOT/EX (Ludwig, 1999).

GEOLOGICAL FINDINGS

In the southern Mawson Escarpment, blocks and lenses of ultramafic to subordinate mafic rocks occur sporadically throughout the metamorphic section. However, in a number of localities, especially at the northern fringe of the Tingey Glacier, they are strongly enriched in steeply dipping, generally east–west trending high-strain shear zones (Fig. 2). These zones were first described by Kamenev et al. (1990) who considered them to represent a tectonic mélange composed of fragments of the Archaean metavolcanic rocks. The high-strain zones occur in general accordance with the structural grain of the Ruker Terrane (Boger et al., 2006). These zones are up to 200 m thick and include highly rounded blocks or lenses of ultramafic and rarely mafic rocks, some 10 cm to 10 metres across, embraced in a matrix of highly sheared or folded gneiss to schist (Fig. 2 a, b). Deformation of the country rock (greyish orthogneiss) strongly increases towards the high-strain shear zones. The matrix contains also much less sheared syn-tectonic granitoid veins (Fig. 2 c). The schistose biotite-quartz-amphibole-plagioclase matrix also contains bands of amphibolite which at least in part formed as strain-induced pressure shadows of reaction rims between ultramafic lenses and the matrix. In a few cases, the concentration of lens-shaped ultramafic to mafic rocks in the high-strain shear zones resembles pillow lava structures (Fig. 2 d) but the strongly sheared matrix of the enclosing metamorphic rock clearly indicates a tectonic origin. Kamenev et al. (1990) reported that up to 50% of these blocks and lenses are rocks of mafic composition (amphibole-plagioclase schist), but our study reveals that the lenses and blocks are predominantly composed of ultramafic rocks.

PETROGRAPHY

Lenses and blocks in the high-strain shear zones from the southern Mawson Escarpment mainly comprise a variety of ultramafic schists, but less metamorphosed and sheared samples were found as well (Fig. 3). The most common rock type is ultramafic amphibolite; less common is amphibole dunite, amphibole orthopyroxenite, harzburgite and also talc–anthophyllite, talc–tremolite and calcite–chlorite–talc schist reported by Kamenev et al. (1990). The rocks consist of different varieties of amphibole (actinolite, tremolite, hornblende or anthophyllite; a detailed investigation of the compositional and microstructural relations of this mineral however is beyond the scope of this study), orthopyroxene and olivine, with secondary talc, serpentine, epidote, phlogopite, carbonate, chlorite, and titanite. The rocks are commonly schistose, although massive varieties also occur, and medium to coarse-grained. Textures are nemato- to lepidogranoblastic, or rarely fibroblastic. A few hornblende–plagioclase mafic schists were also found. Representative chemical analyses of the rock-forming minerals are presented in table 1. In the following, some ultramafic rocks are described in detail.

Highly retrogressed ultramafic schist NRL 160 (Fig. 3 a, b) is a heterogranular rock. It consists of pseudomorphs after mafic minerals which

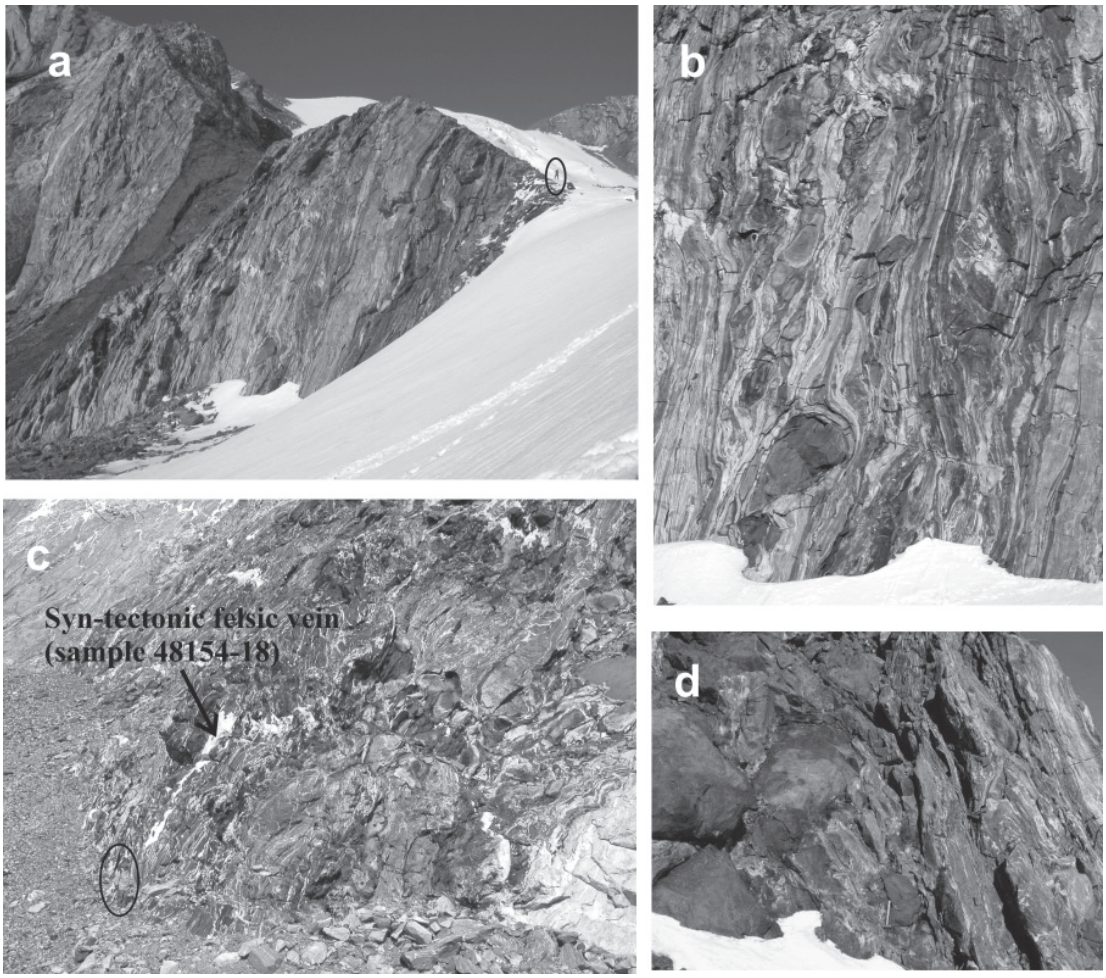

Fig. 2 - High-strain shear zone at the northwestern fringe of Tingey Glacier, southern Mawson Escarpment. a) General view with abundant ultramafic blocks and lenses. The shear zone is cut by a presumably Proterozoic mafic dyke (note person in the upper right for scale). b) Detail of fig. 2a showing lenses of different ultramafic rocks in a heterogenous schistose matrix (horizontal view area about 15 m). c) Syn-tectonic granitic vein in a high-strain shear zone from NE Tingey Glacier (note person in the lower left for scale). Mafic rock sPCM62.5 and schistose orthogneiss sPCM 62.8 were also sampled at this site. d) Rounded blocks of ultramafic rock resembling "pillow" structure (scale is given by a hammer in the low central area).

were up to 1–1.5 mm large and orthopyroxene grains (altogether 70–75 vol.-%) enclosed in a finer-grained matrix of fibrous aggregates of talc, amphibole (anthophyllite and calcic amphibole), carbonate, and chlorite. The pseudomorphs are made up by dust of opaque minerals, talc, amphibole, and chlorite. Orthopyroxene has a molar $100*Mg^{+2}/Mg^{+2}+Fe^{+2}$ ("mg") of 83–85 and contains 0.9–1.0 wt.-% Al_2O_3 (Tab. 1); few analyses reveal less magnesian compositions (mg = 74.5–75.5) with higher Al_2O_3 contents (up to 1.8 wt.-%) and somewhat lower Cr_2O_3 contents. Olivine ($Fo_{68–77}$) occurs rarely as inclusions or in contact to orthopyroxene. Orthopyroxene as well as the precursor mineral(s) of the dusty pseudomorphs may represent highly resorbted phenocrysts. One large orthopyroxene grain (5 mm across) may be interpreted as a xenocryst.

Olivine-amphibole-orthopyroxenite NRL 180a (Fig. 3 c, d) is a coarse-grained rock with glomeroblastic texture. Orthopyroxene (30-60 vol.-%) forms up to 4–5 mm large poikiloblasts. Olivine (Fo_{89}, 30-40 vol.-%) forms large rounded and fractured grains or small inclusions in orthopyroxene. Colourless or slightly greenish-grey amphibole (actinolite, up to 5 vol.-%) forms small (< 0.5 mm) laths. Slightly brownish, nearly colourless phlogopite (mg = 93–94; 5-25 vol.-%) forms dispersed flakes which apparently represent small porphyroblasts. Low-Cr spinel (Cr_2O_3 13–14 wt.-%) forms abundant small isometric crystals of greenish-brown to brown colour. It occurs interstitially and also as inclusions in amphibole.

Amphibole orthopyroxenites sPCMMcue 2, NRL 180b (Fig. 3 e, f) and NRL 181 are texturally similar, but instead of olivine granoblastic, isometric colourless amphibole is found. NRL 181 has granoblastic heterogranular (poikiloblastic) or possibly apoheteradcumulate texture. Coarse (up to 6–7 mm) prismatic orthopyroxene (mg 87.5–88.0) crystals (50 vol.-%) are surrounded by nearly polygonal aggregates of finer-grained colourless amphibole (actinolite, optically positive, 40 vol.-%). Pale brown phlogopite (mg = 93–94; laths up to 1.0–1.5 mm or numeral grains, 10 vol.-%) is present as inclusions in orthopyroxene or fills in the interstitials. Orthopyroxene also contains abundant small inclusions of colourless amphibole.

Retrogressed dunite NRL 185 is a medium- to fine-grained rock of lepidoblastic texture with relict

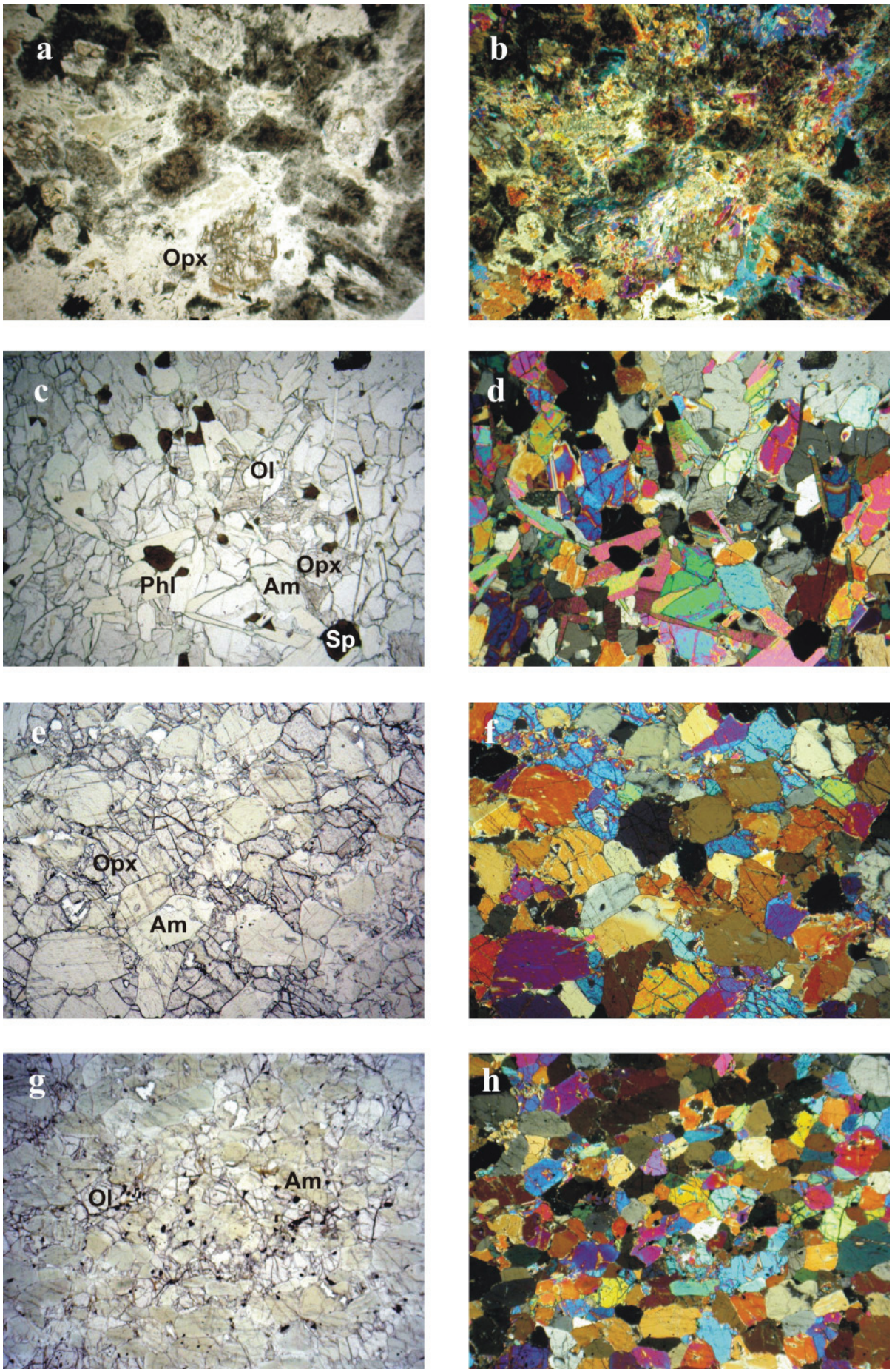

Fig. 3 - Microphotographs of ultramafic rocks from the southern Mawson Escarpment: a, b) ultramafic schist NRL 160; c, d) olivine–amphibole-bearing orthopyroxenite NRL 180a; e, f) amphibole-bearing orthopyroxenite NRL 180b; g, h) olivine–orthopyroxene-bearing amphibolite sPCMMcue4. a, c, e, g parallel polar light , in b, d, f, h crossed polar light. View area 7.5 x 5 mm.

Tab. 1 - Compositions of selected rock-forming minerals of ultramafic and mafic rocks from high-strain shear zones of the southern Mawson Escarpment as determined by microprobe analysis.

Sample#	*NRL160*	*NRL160*	*NRL160*	*NRL180a*	*NRL180a*	*NRL160*	*NRL160*	*NRL160*	*NRL160*	*NRL180a*	*NRL180a*
Note	Ol	Ol	Ol	Ol	Ol	Opx	Opx	Opx	Opx	Opx	Opx
SiO_2	38.93	39.45	38.34	41.01	41.25	56.19	56.11	56.12	54.17	57.05	57.44
TiO_2	0.03	0.04	0.02	0.01		0.20	0.22	0.21	0.48	0.03	0.03
Al_2O_3	0.01		0.00	0.00	0.00	0.83	0.99	0.79	1.80	1.90	1.80
Cr_2O_3	0.01		0.00		0.01	0.54	0.58	0.43	0.17	0.09	0.13
FeO	23.24	21.03	26.70	10.41	10.44	10.97	9.06	10.13	15.65	7.22	7.13
MnO	0.34	0.27	0.42	0.16	0.14	0.21	0.17	0.22	0.28	0.17	0.21
NiO	0.28	0.36	0.36	0.50	0.53	0.11	0.13	0.15	0.05	0.09	0.10
MgO	37.69	39.54	34.48	48.38	47.94	29.11	30.94	29.84	25.98	34.02	33.57
CaO	0.01	0.01	0.00	0.02	0.01	2.39	1.86	2.29	1.55	0.17	0.09
Na_2O	0.01	0.00	0	0.00	0.01	0.09	0.12	0.11	0.04	0.00	0.00
K_2O	0.00	0.00	0.02	0.00	0.00			0.01	0.01	0.00	0.00
Total	100.53	100.70	100.34	100.49	100.34	100.65	100.18	100.32	100.19	100.73	100.50
Oxygen	4.00	4.00	4.00	4.00	4.00	6.00	6.00	6.00	6.00	6.00	6.00
Si	1.01	1.01	1.02	1.00	1.01	1.98	1.97	1.98	1.96	1.96	1.97
Ti	0.00	0.00	0.00	0.00	0.00	0.01	0.01	0.01	0.01	0.00	0.00
Al	0.00	0.00	0.00	0.00	0.00	0.03	0.04	0.03	0.08	0.08	0.07
Cr	0.00	0.00	0.00	0.00	0.00	0.02	0.02	0.01	0.00	0.00	0.00
Fe3+	0.00	0.00	0.00	0.00	0.00	0.00	0.00	0.00	0.00	0.00	0.00
Fe2+	0.50	0.45	0.59	0.21	0.21	0.32	0.27	0.30	0.47	0.21	0.20
Mn	0.01	0.01	0.01	0.00	0.00	0.01	0.01	0.01	0.01	0.00	0.01
Ni	0.01	0.01	0.01	0.01	0.01	0.00	0.00	0.00	0.00	0.00	0.00
Mg	1.46	1.51	1.36	1.77	1.75	1.53	1.62	1.57	1.40	1.74	1.72
Ca	0.00	0.00	0.00	0.00	0.00	0.09	0.07	0.09	0.06	0.01	0.00
Na	0.00	0.00	0.00	0.00	0.00	0.01	0.01	0.01	0.00	0.00	0.00
K	0.00	0.00	0.00	0.00	0.00	0.00	0.00	0.00	0.00	0.00	0.00
P	0.00	0.00	0.00	0.00	0.00	0.00	0.00	0.00	0.00	0.00	0.00
Total	2.99	2.99	2.98	3.00	2.99	3.99	4.00	4.00	3.99	4.00	3.99
Mg#	74.30	77.03	69.71	89.23	89.11	82.55	85.89	84.00	74.74	89.37	89.36

medium-grained adcumulate texture. Medium-grained olivine (65-70%) forms strongly fractured isometric "resorbed" rounded grains (0.5–2.0 mm) enclosed in a matrix of finer-grained phlogopite, chlorite and talc aggregates (30 vol.-%). Rare opaque minerals form small, irregularly-shaped grains in phlogopite.

Orthopyroxene amphibolite (sPCM-Ting 3, olivine amphibolite (sPCMTing 2, sPCMTing 3, sPCMMCue 5), and olivine-orthopyroxene-amphibolite (sPCMMCue4; Fig. 3 g, h) are fine-grained rocks with heterogranular (mostly <0.5 mm, with some larger crystals) granoblastic or apoheteradcumulate texture. The rock are composed of olivine (30-45 vol.-%) and colourless to very pale green amphibole (50-70 vol.-%) which forms nearly polygonal fabrics with low-energy grain boundaries. Phlogopite flakes of similar size occur in some domains. Rare orthopyroxene and magnetite grains randomly occur.

Amphibolite (sPCM 64.2, sPCM 68.2, sPCMTing 4) has a fibrous or poorly developed fine-grained massive nematoblastic texture. Relict granoblastic texture is sometimes also present. The samples comprise a mass of fibrous pale green (sPCM 64.2, sPCM 68.2) or colourless (sPCMTing 4) amphibole, along with chlorite and phlogopite in varying proportions. Opaque mineral dust delineates pseudomorphs after mafic minerals, as in part do mica flakes. Some pseudomorphs have a brownish tint due to the colour of the secondary minerals, and may exhibit dusty stripes which run along the elongation and which may be "shadow" pyroxene exsolution lamellae.

Mafic hornblende–plagioclase schist (sPCM 61.2, 62.5, and 69.4) is a fine- or medium-grained rock of granoblastic or lepidogranoblastic texture and massive to schistose structure. Hornblende accounts for 60–70 vol.-%. Biotite and titanite are the minor constituents.

The rocks apparently have been overprinted by two metamorphic events. The earlier event is exhibited by colourless to pale green amphibole and spinel formed subsequent to pyroxene, olivine and spinel crystallisation. However, amphibole contains no relics of primary minerals while the other rock-forming minerals (orthopyroxene and olivine) do not show any metamorphic reaction. In some rocks, amphibole with polygonal grain shape occurs in equilibrium with (primary) olivine and orthopyroxene. The later event is reflected by widespread occurrence of fibrous colourless amphibole, hornblende and also chlorite, talc, opaque minerals. Phlogopite seems to have crystallized at this stage and it is not altered. This stage occurred under varying stress conditions which led to formation of a variety of transitional textures from homogeneous fibrous (no shear) to strongly schistose nematoblastic (high shear) with formation of coarse amphibole porphyroblasts.

Tab. 1 - Continued.

Sample	*NRL180b*	*NRL180b*	*NRL181*	*NRL181*	*NRL180a*	*NRL180a*	*NRL180b*	*NRL180b*	*NRL180b*	*NRL180b*
Note	Opx	Opx	Opx	Opx	Sp	Sp	Am	Am	Bt	Bt
SiO_2	57.87	57.60	58.12	58.08	0.02	0.00	55.70	55.51	41.78	42.02
TiO_2	0.05		0.01		0.02	0.04	0.04	0.06	0.35	0.36
Al_2O_3	0.51	0.53	0.45	0.51	50.87	51.89	3.69	4.16	13.76	13.66
Cr_2O_3	0.07	0.08	0.09	0.07	14.36	13.47	0.47	0.38	0.66	0.80
Fe_2O_3										
FeO	8.84	8.85	8.14	8.42	15.16	15.22	2.79	2.75	2.96	2.78
MnO	0.16	0.19	0.18	0.18	0.08	0.10	0.07	0.04	-0.02	0.03
NiO	0.10	0.09	0.14	0.13	0.41	0.38	0.23	0.18	0.37	0.37
MgO	32.23	32.44	33.46	33.20	16.94	16.57	21.42	21.60	23.68	23.64
CaO	0.25	0.22	0.26	0.23	0.01		12.41	12.55		
Na_2O	0.01			0.02		0.01	0.71	0.84	0.49	0.51
K_2O	0.01	0.01	0.01	0.00	0.01		0.13	0.15	9.26	9.32
Total	100.11	99.98	100.84	100.80	97.86	97.69	97.66	98.24	93.33	93.49
Oxygen	6.00	6.00	6.00	6.00	3.00	3.00	23.00	23.00	22.00	22.00
Si	2.01	2.00	2.00	2.00	0.00	0.00	7.67	7.60	5.98	6.00
Ti	0.00	0.00	0.00	0.00	0.00	0.00	0.00	0.01	0.04	0.04
Al	0.02	0.02	0.02	0.02	1.24	1.26	0.60	0.67	2.32	2.30
Cr	0.00	0.00	0.00	0.00	0.23	0.22	0.05	0.04	0.07	0.09
Fe3+	0.00	0.00	0.00	0.00	0.00	0.00	0.00	0.00	0.00	0.00
Fe2+	0.26	0.26	0.23	0.24	0.26	0.26	0.32	0.31	0.35	0.33
Mn	0.00	0.01	0.01	0.01	0.00	0.00	0.01	0.00	0.00	0.00
Ni	0.00	0.00	0.00	0.00	0.01	0.01	0.03	0.02	0.04	0.04
Mg	1.67	1.68	1.72	1.71	0.52	0.51	4.40	4.41	5.06	5.04
Ca	0.01	0.01	0.01	0.01	0.00	0.00	1.83	1.84	0.00	0.00
Na	0.00	0.00	0.00	0.00	0.00	0.00	0.19	0.22	0.14	0.14
K	0.00	0.00	0.00	0.00	0.00	0.00	0.02	0.03	1.69	1.70
Total	3.98	3.98	3.99	3.99	2.26	2.26	15.11	15.16	15.70	15.68
Mg#	86.66	86.73	87.99	87.55			93.20	93.35	93.44	93.80

Mineral abbreviations after Kretz (1983), Am – amphibole.

GEOCHEMISTRY

The chemical composition of the ultramafic rocks (Tab. 2) varies considerably, especially in respect to their concentrations of Fe_2O_3* (4-15 wt.-%), MgO (17-30 wt.-%), CaO (5-12 wt.-%), and some trace elements (Cr 600-3500 ppm, Ni 200-1700 ppm, Co 50-100 ppm, Zr up to 80 ppm, Sr up to 150 ppm, Cu up to 40 ppm, in one sample 400 ppm). Variability of SiO_2 content is more restricted (46-54 wt.-%). TiO_2 (0.1-0.4 wt-%), Al_2O_3 (<9 wt-%), and P_2O_5 (<0.1 wt-% with one exception) contents are generally low. Alkalis vary in relatively narrow ranges: Na_2O 0.2-1.0 wt-%, K_2O 0.1-1.2 wt-% with only a few exceptions. Rb is also generally high (10-100 ppm). Accordingly, relevant major and trace element ratios scatter in very wide ranges: Al_2O_3/TiO_2 is mostly 10–60, CaO/TiO_2 15–80, CaO/Al_2O_3 0.7–3.5, Zr/Y 2–8, Ti/Zr 80–120, TiO_2/P_2O_5 4–17. Index mg (mg = 100·MgO/(MgO+FeO), molecular) varies considerably in the range of 70-90 reflecting compositions of the rock suite transitional between typical ultramafic rocks from the upper mantle (mg $\geq$ 90) and primitive basaltic rocks (mg $\leq$ 70). A very similar conclusion can be drawn based on other element abundances (*e.g.*, Cr, Ni). The chemical composition of two gneisses sampled from a shear zone at NE Tingey Glacier (sPCM 62.8) and from close to a shear zone at Rimmington Bluff (sPCM 69.6) are given for comparison and will not be discussed in detail. Their trace element compositions indicate that sPCM 69.6 and sPCM 62.8 can be correlated with high-Y and low-Y groups of orthogneisses, respectively, from elsewhere in the Ruker Province (Mikhalsky et al. 2006b).

In terms of the total alkalis–silica classification of magmatic rocks by Le Maitre (1989) most samples are sub-alkaline and plot in the komatiite or picrite

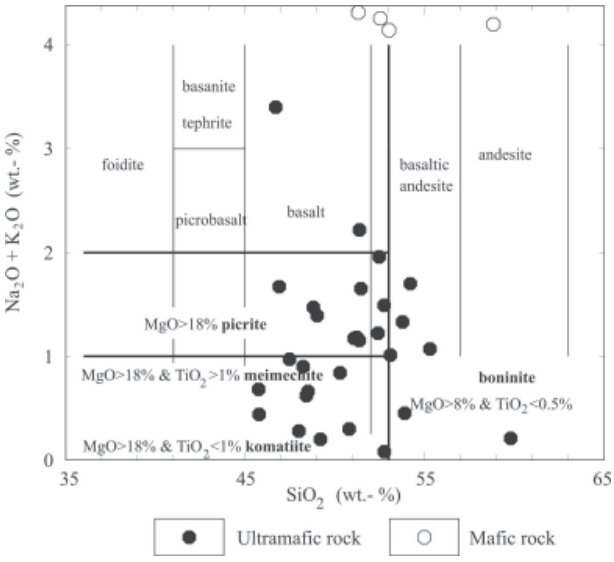

Fig. 4 - SiO_2 vs (Na_2O+K_2O) classification diagram after Le Maitre (1989) for ultramafic and mafic rocks from the southern Mawson Escarpment.

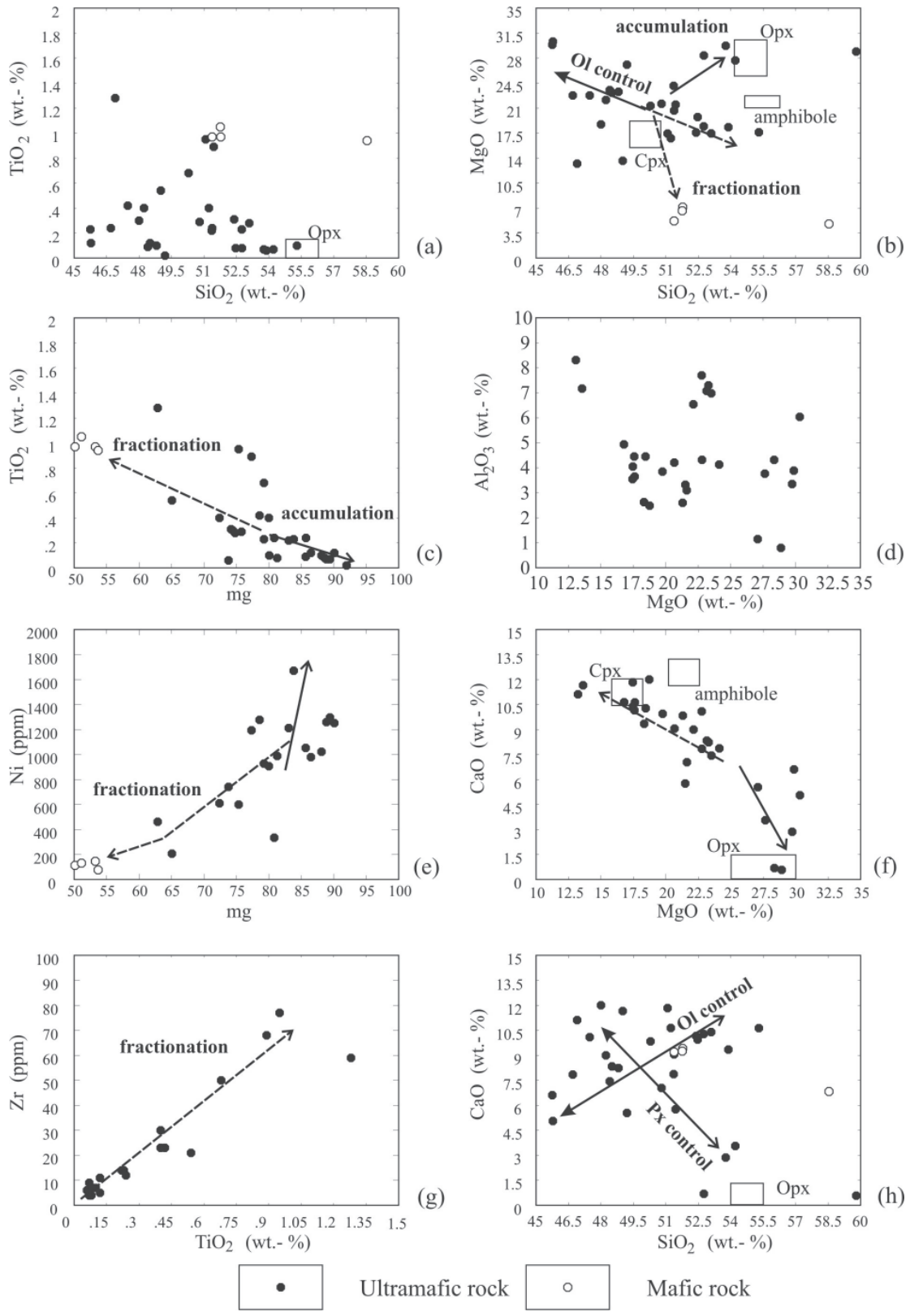

Fig. 5 - Selected major and trace element plots for the ultramafic and mafic rocks from the southern Mawson Escarpment. Squares indicate the composition of the rock-forming minerals (Opx, Am – measured, Cpx – common composition; compare text for details).

fields (Fig. 4). In binary major and trace element plots (Fig. 5 a - h), these rocks form consistent trends, although only few plots show really good element correlation (*e.g.*, mg vs Ni, MgO vs CaO, TiO_2 vs Zr; Fig. 5 e, f, g). TiO_2 tends to form a convex trend when plotted against SiO_2 with maximum TiO_2 abundances reached at about 50 wt.-% SiO_2. Assuming a co-magmatic origin of the rocks, this may be explained by initial olivine+pyroxene fractionation with magnetite joining the cotectic assemblage at a later stage. However, some of the high-silica samples are rich in orthopyroxene and may thus be interpreted as cumulates. This is also evident from the MgO–CaO plot (Fig. 5 f). MgO plotted against SiO_2 seems to

Tab. 2 - Representative chemical analyses of ultramafic and mafic rocks and two orthogneisses from high-strain shear zones of the southern Mawson Escarpment. Major and trace elements unless otherwise stated: determined by XRF; REE, Nb, Ta, Hf, U, Th and Pb by ICP-MS.

Sample	*sPCM Ting2*	*sPCM 64.2*	*sPCM Ting4*	*sPCM Ting3*	*NRL 160*	*sPCM 68.2*	*sPCM Mcue2*	*sPCM 69.4*	*NRL 181*	*NRL 180b*	*sPCM 62.8*	*sPCM 69.6*
Lithology	*Ol amphi-bolite*	*Amphi-bolite*	*Amphi-bolite*	*Ol amphi-bolite*	*Ultra-mafic schist*	*Amphi-bolite*	*Am orthpy-roxenite*	*Mafic Am–Pl schist*	*Am orthopy-roxenite*	*Am orthopy-roxenite*	*Schistose Ortho-gneiss*	*Ortho-gneiss*
SiO_2	45.78	46.90	48.51	49.01	50.29	51.08	51.36	51.78	53.77	54.21	70.41	69.23
TiO_2	0.12	1.28	0.12	0.54	0.68	0.95	0.22	0.97	0.07	0.07	0.38	0.54
Al_2O_3	6.04	8.31	7.08	7.15	2.60	3.55	4.13	12.24	3.34	3.78	15.30	12.82
Fe_2O_3*	6.60	15.46	7.17	14.48	11.04	11.30	9.73	12.40	6.96	6.86	2.79	6.61
MnO	0.12	0.26	0.14	0.28	0.18	0.16	0.17	0.19	0.14	0.10	0.03	0.10
MgO	30.33	13.23	23.16	13.62	21.31	17.45	24.13	7.14	29.73	27.67	0.84	0.16
CaO	5.06	11.12	8.34	11.66	9.84	11.84	7.87	9.41	2.87	3.56	2.79	2.60
Na_2O	0.37	1.01	0.57	0.88	0.68	1.07	0.38	3.58	0.25	0.37	5.21	3.85
K_2O	0.07	0.66	0.09	0.51	0.16	0.10	0.77	0.98	1.08	1.33	1.35	3.30
P_2O_5	0.01	0.38	0.02	0.04	0.04	0.07	0.01	0.15	0.02	0.01	0.11	0.08
LOI	4.61	0.69	3.92	1.14	1.94	1.29	0.34	0.58	1.07	1.16	0.45	0.06
sum	99.11	99.3	99.12	99.31	98.76	98.86	99.11	99.42	99.3	99.12	99.67	99.45
V	108	253	108	305	122	152	121	186	52	84	21	12
Cr	3156	677	2004	740	3415	3473	1961	525	1771	2162	18	8
Ni	1252	463	980	207	928	600	1212	146	1297	1260	5	5
Cu	bdl	bdl	12	11	400	451	26	bdl	bdl	bdl	16	22
Zn	50	138	58	153	87	89	68	186	88	65	66	167
Ga	4	14	5	14	5	6	7	nd	nd	4	22	19
Rb	10	37	7	18	10	8	60	30	76	103	50	55
Sr	29	47	15	10	109	145	60	276	7	15	304	183
Y	bdl	9	bdl	13	4	10	7	26	5	bdl	bdl	33
Zr	5	59	11	21	50	77	14	114	9	4	210	553
Nb	bdl	22.0	0.3	2.5	3.0	3.0	1.1	6.6	2.0	0.6	7.3	20.3
Ba	bdl	96	bdl	18	30	13	16	261	23	77	156	1922
La	0.36	28.40	0.84	3.58	8.85	32.30	0.88	12.20	nd	1.22	23.6	28.7
Ce	0.63	53.10	2.22	9.49	21.20	52.60	2.16	27.20	nd	2.41	42.2	60.3
Pr	0.09	6.02	0.30	1.33	2.92	5.44	0.33	3.55	nd	0.24	4.42	7.76
Nd	0.49	20.20	1.44	6.42	12.00	19.00	1.96	14.90	nd	0.74	15.0	31.7
Sm	0.18	3.68	0.40	1.85	2.84	3.95	0.64	3.90	nd	0.13	2.74	7.77
Eu	0.08	1.56	0.17	0.71	0.83	1.05	0.18	1.37	nd	0.10	0.80	3.97
Gd	0.38	3.43	0.57	2.62	2.59	3.69	1.00	4.18	nd	0.29	2.05	8.11
Tb	0.09	0.48	0.12	0.51	0.38	0.51	0.20	0.75	nd	0.07	0.29	1.40
Dy	0.71	2.62	0.92	3.36	1.94	2.64	1.31	4.68	nd	0.53	1.35	8.11
Ho	0.17	0.51	0.23	0.71	0.35	0.47	0.27	0.96	nd	0.13	0.23	1.64
Er	0.57	1.48	0.76	2.06	0.92	1.21	0.81	2.80	nd	0.43	0.59	4.82
Tm	0.09	0.22	0.12	0.31	0.13	0.16	0.12	0.41	nd	0.07	0.07	0.71
Yb	0.63	1.42	0.87	1.94	0.74	1.00	0.77	2.59	nd	0.47	0.43	4.72
Lu	0.10	0.22	0.13	0.27	0.10	0.14	0.11	0.39	nd	0.07	0.07	0.83
Hf	0.20	1.50	0.30	0.80	1.40	2.00	0.40	3.10	bdl	0.20	5.60	12.1
Ta	bdl	1.61	0.02	0.25	0.33	0.52	0.42	0.47	bdl	bdl	0.43	1.16
Pb	bdl	bdl	bdl	12	8	bdl	bdl	8	bdl	9	16	10
Th	0.05	2.58	0.13	0.57	0.81	1.78	0.11	0.96	nd	0.26	4.52	3.50
U	0.01	0.50	0.06	0.53	0.21	0.31	0.49	0.28	nd	0.12	0.36	0.70
mg	90.10	62.89	86.48	65.07	79.26	75.36	83.08	53.28	89.43	88.87	37.35	4,57
CaO/TiO_2	42.17	8.69	69.50	21.59	14.47	12.46	35.77	9.70	41.00	50.86	7.34	12.24
CaO/Al_2O_3	0.84	1.34	1.18	1.63	3.78	3.34	1.91	0.77	0.86	0.94	0.18	0.52
Zr/Y		6.56		1.62	12.50	7.70	2.00	4.47	1.80			16.76
Ti/Zr	143.88	130.06	65.40	154.16	81.53	73.96	94.21	51.01	46.63	104.91	10.85	5.85
Zr/Nb		2.68	36.67	8.40	16.67	25.67	12.73	17.27	4.50	6.67	28.78	27.24
Ti/P	16.48	4.63	8.24	18.54	23.35	18.64	30.22	8.88	4.81	9.61	4.75	9.27

Fe_2O_3* – total Fe as Fe_2O_3. bdl – below detection level. mg see in the text, nd – no data.

form an isometric field, which may reflect combined olivine and pyroxene control. Relatively high-CaO rocks may reflect clinopyroxene accumulation, although clinopyroxene was detected only in one rock from this area. These compositions are mostly represented by rocks rich in Ca-amphibole. TiO_2 and Zr, plotted against mg both show very similar distribution patterns with slight increase at the decrease of mg. Some samples have somewhat elevated Ti and Zr contents (at mg = 74–80) probably due to fractionation or rather accumulation of magnetite (which could have been replaced during metamorphism). There is a good correlation between Mg and Ni which apparently reflects a strong olivine control. CaO also shows good negative correlation with Mg.

In a primitive mantle-normalized trace element diagram (Fig. 6), the ultramafic to mafic rocks from the southern Mawson Escarpment display consistent but highly fractionated patterns. The high-field strength elements (HFSE: P, Zr, Ti, Y, Nb) mostly scatter between 0.3-7.0 (primitive mantle normalized) and thus basically display element concentrations similar to the primitive mantle. Except for a few samples discussed below no obvious negative Nb anomaly is evident. Three samples (retrogressed ultramafic schist NRL 160 and ultramafic amphibolites sPCM 64.2, sPCM 68.2) are somewhat enriched in most trace elements (except Y). These samples also show a negative Sr anomaly and less evident negative Nb–Ta anomalies. In addition, the large-ion lithophile elements (LILE) Pb, Rb, Th, U, K show a considerable enrichment mostly in the range of 10-100 (primitive mantle normalized). Mafic rocks display spiderdiagram patters quite similar to the "enriched" ultramafic rocks with a moderate negative Nb anomaly, but differ in having a prominent negative Ti anomaly which may due to magnetite fractionation.

Chondrite-normalized rare-earth element distribution patterns show considerable variance (Fig. 7). Three samples (sPCM Ting3, sPCM Mcue2, sPCM Ting4) shows a nearly uniform flat distribution pattern with $(La/Yb)_N$ ratio close to 1. Two samples (NRL 180b, sPCMTing2) have a negative inclination in their patterns for the middle to heavy REE as reflected in values for $(Sm/Yb)_N$ well below unity (0.3–0.5). Among these, NRL 180b shows a strong enrichment of the light REE with $(La/Sm)_N$ = 6.1. Concave REE patterns like that of NRL 180b may be explained by an early light to middle REE depletion event for instance in the course of melt extraction superimposed by a secondary metasomatic re-enrichment of the light REE.

Three samples (NRL 160, sPCM 64.2, sPCM 68.2) show light to middle REE enriched patterns with $(La/Yb)_N$ in the range 9–23 similar to incompatible-enriched basaltic rocks of within-plate geotectonic setting. Two mafic rocks (sPCM 62.5, sPCM 69.4) have overall higher REE abundances (about 20 times chondritic) and a moderate light REE enrichment with $(La/Yb)_N$ ~3, and $(La/Sm)_N$ ~2.

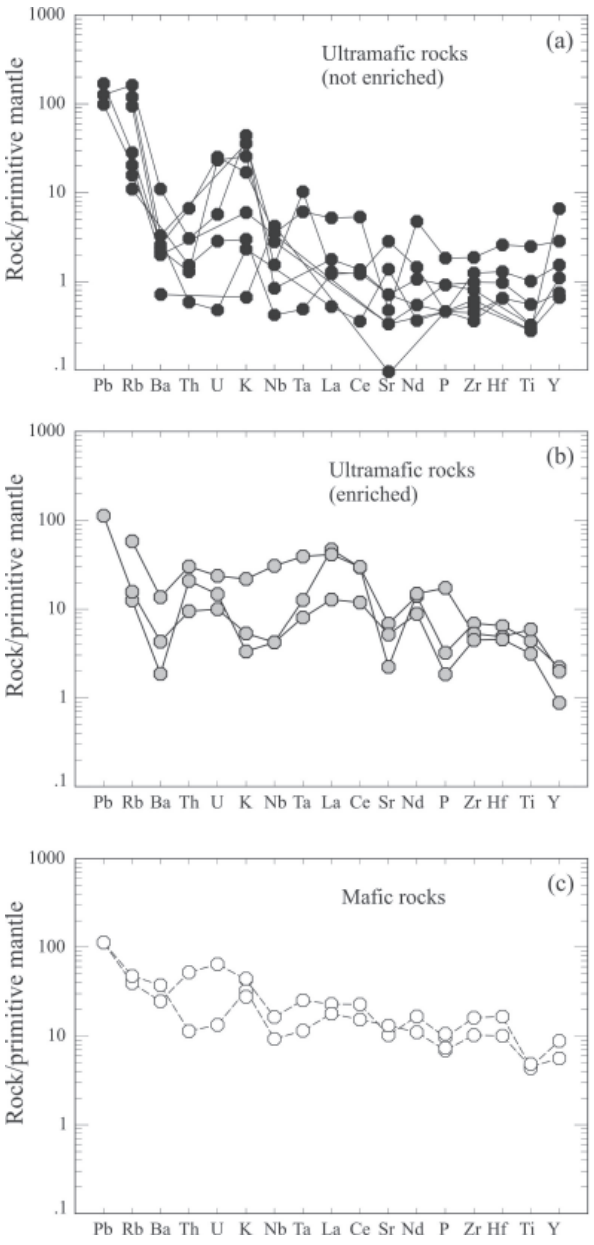

Fig. 6 -Primitive mantle-normalized trace element abundance diagram for ultramafic and mafic rocks from high-strain shear zones of the southern Mawson Escarpment. Normalization factors from Sun & McDonough (1989). (a) ultramafic rocks that are not enriched; (b) enriched ultramafic rocks; (c) mafic rocks.

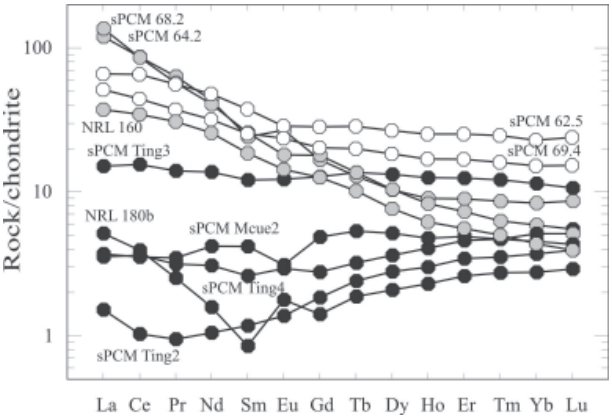

Fig. 7 - Chondrite normalised REE abundances diagram for ultramafic and mafic rocks from the southern Mawson Escarpment. Normalization factors from Sun & McDonough (1989).

Tab. 3 - Sm–Nd isotope data for ultramafic to mafic rocks and two orthogneisses from high-strain shear zones of the southern Mawson Escarpment. (WR: whole rock; Sm and Nd: concentrations in ppm; ε_{Nd} (t): calculated for an age of 3.3 Ga; T_{Nd} and T_{CHUR} in Ga; for calculation of f see text).

Sample	*Material*	*Lithology*	*Locality*	*Sm*	*Nd*	$^{147}Sm/^{144}Nd$	$^{143}Nd/^{144}Nd$	$\varepsilon_{Nd}(0)$	ε_{Nd} (t)	T_{DM}	T_{CHUR}	*f*
sPCM 61.2	WR	Mafic Hbl–Pl schist	Philpot Bluff	4.100	13.72	0.1807	0.512646	0.2	7.0	2.33	-0.08	-0.08
sPCM 64.2	WR	Amphibiolite	McCue Bluff	3.943	23.14	0.1026	0.511603	-20.2	20.0	2.12	1.67	-0.48
sPCM 68.2	WR	Retrogressed amphibolite	McCue Bluff	5.151	26.50	0.1171	0.511538	-21.5	12.5	2.54	2.10	-0.40
sPCMMcue2	WR	Am-orthpyroxenite	McCue Bluff	0.600	1.571	0.2300	0.513296	12.8	-1.3	1.35	2.99	0.17
sPCMTing2	WR	Retrogressed Ol-amphibolite	NW Tingey Glacier	0.155	0.352	0.2647	0.514559	37.5	8.6	4.16	4.26	0.35
sPCM 62.5	WR	Retrogressed mafic Ttn-bearing Hbl–Pl schist	NE Tingey Glacier	6.545	26.49	0.1493	0.511478	-22.6	-2.5	3.93	3.70	-0.24
sPCM 62.8	WR	Schistose orthogneiss	NE Tingey Glacier	2.739	15.46	0.1071	0.510681	-38.2	0	3.51	3.30	-0.24
NRL 160	WR	Retrogressed ultramafic schist	Rimmington Bluff	2.684	12.13	0.1332	0.511631	-19.6	7.4	2.86	2.41	-0.32
NRL 180b	WR	Phl-bearing Am-orthopyroxenite	Rimmington Bluff	0.130	0.582	0.1341	0.511508	-22.0	4.6	3.13	2.74	-0.32
sPCM 69.4	WR	Retrogressed mafic Hbl–Pl schist	Rimmington Bluff	4.032	16.49	0.1477	0.511588	-20.5	0.4	3.58	3.24	-0.25
sPCM 69.6	WR	Orthogneiss	Rimmington Bluff	8.443	36.67	0.1391	0.511395	-24.3	0.3	3.56	3.27	-0.25
NRL181	WR	Phl-bearing Am orthopyroxenite	Dalton Corner	1.534	5.379	0.1725	0.511933	-13.8	-3.5	4.47	4.39	-0.12
NRL181	Cpx		Dalton Corner	0.260	0.513	0.3064	0.515361	53.1	6.5	3.60	3.75	0.56

SM-ND ISOTOPES

All but two ultramafic and mafic rocks have highly variable negative Sm/Nd ratios ($f_{Sm/Nd}$ = -0.48 – -0.08, where $f_{Sm–Nd} = (^{147}Sm/^{144}Nd_{sample}/^{147}Sm/^{144}Nd_{CHUR}) - 1$), single-stage depleted-mantle model ages (T_{DM}) between 2.1–4.5 Ga and $\varepsilon_{Nd}(0)$ values between 0 – -23 (Tab. 3). The sample with a $f_{Sm–Nd}$ value of -0.12 (NRL 181) probably represents a reasonably unfractionated rock. Clinopyroxene separated from this sample yields a mineral-WR age of *ca.* 3.9 Ga with $\varepsilon_{Nd}(t)$ = -2. We refer these values to the approximate age when the rock was formed in the upper mantle and to its initial Nd isotope composition, respectively. The other rocks likely experienced Sm–Nd fractionation during an unknown number of subsequent igneous or metasomatic events which led to the large scatter in $f_{Sm–Nd}$ and T_{DM} values. Two samples (sPCMMcue2, sPCMTing2) have very high $f_{Sm/Nd}$ and T_{CHUR} model ages of ca 3.0 and 4.3 Ga pointing to the presence of a specific depleted source region (*c.f.* Bennett et al. 2003).

U–Pb DATING

U–Pb zircon ages were obtained by SHRIMP techniques for a syn-tectonic granitic vein (sample 48154-18) which intruded a high-strain shear zone with ubiquous mafic/ultramafic lenses and blocks located in the north-eastern Tingey Glacier area. The U–Pb data are presented in table 4.

Sample 48154-18 represents a thin leucocratic quartz–feldspar vein (Fig. 2 c). The zircon grains recovered from this sample are slightly brownish or pinkish in colour, elongated prismatic in shape (normally the ratio grain length/width l = 3 – 4, but pencil-like grains also occur), with rounded terminations; they are somewhat fractured and have clearly developed oscillatory zoning and cores (Fig. 8a). The cores are very dark in cathodoluminescene images (CL) due to high U content and did not yield reliable analyses. Seven analyses on zoned areas of seven grains were obtained. The Th/U ratio is fairly uniform in the range 0.12–0.18. All analyses are highly discordant and tend to plot closer to the lower interception of the discordia with the Concordia (Fig. 8b). Six out of seven analyses form a regression line with an upper intercept age of 3333+/-60 Ma and a lower intercept age of 2539+/-61 Ma (MSWD = 0.67). The seventh analysis is slightly more discordant and may contain somewhat older inherited material or may have undergone more pronounced Pb lost during later events.

DISCUSSION

GEOCHEMICAL CONSIDERATIONS

Many of the geochemical features of the ultramafic to mafic blocks and lenses in the high-strain shear zones of the southern Mawson Escarpment, such as strong positive correlation between Ti – Zr and negative correlations between Mg – TiO_2 and Mg – Zr may be attributed to a control by ferromagnesian minerals (olivine, pyroxenes) in the course of magmatic fractionation processes. Olivine control is best evidenced by correlation between Ni and Mg (Fig. 5e). These features led Kamenev et al. (1990) to suggest a volcanic origin of these rocks, which were tentatively ascribed to form part of a komatiite suite. Indeed, these rocks plot mostly within the peridotite

Tab. 4 - U–Pb isotope ion-microprobe data (SHRIMP) on zircons from granitoid syntectonic vein 48154-18 from a high-strain shear zone of the southern Mawson Escarpment

Grain	U	Th	$^{232}Th/^{238}U$	$^{206}Pb^*$	Ages (Ma)					Radiogenic ratios						
spot	(ppm)	(ppm)		(ppm)	$^{206}Pb/^{238}U$		$^{207}Pb/^{206}Pb$		D (%)	$^{207}Pb^*/^{206}Pb^*$		$^{207}Pb^*/^{235}U$		$^{206}Pb^*/^{238}U$		err corr
											±%		±%		±%	
3.1	443	72	0.17	194	2655	±12	2719.0	±8.1	2	0.18770	0.45	13.164	0.75	0.5096	0.56	0.76
5.1	457	77	0.18	208	2737	±12	2845.5	±7.4	4	0.20376	0.42	14.76	0.71	0.5290	0.55	0.77
2.1	711	107	0.16	344	2876.5	± 8.9	3051.1	±5.5	6	0.23163	0.31	17.824	0.51	0.5624	0.38	0.74
7.1	474	64	0.14	231	2890	±11	2982.3	±6.2	3	0.22033	0.39	17.17	0.61	0.5656	0.47	0.77
6.1	645	81	0.13	318	2922.2	± 9.5	3033.6	±6.8	4	0.22755	0.42	17.98	0.59	0.5735	0.40	0.69
4.1	556	64	0.12	283	3003	±16	3104.8	±5.6	3	0.23771	0.35	19.45	0.74	0.5934	0.65	0.88
1.1	570	79	0.14	295	3043	±10	3136.9	±5.4	3	0.24288	0.33	20.18	0.55	0.6033	0.42	0.78

D (%; discordance): 100 * { [age $^{207}Pb/^{206}Pb$] / [age$^{206}Pb/^{238}U$] - 1}; Errors are 1-sigma. Pb* indicates the radiogenic portion; error in standard calibration was 0.32%.

komatiite field in the cation classification diagram of Jensen (1976) (Fig. 9 b). However, most of the major and trace element ratios (*e.g.*, Ca/TiO_2, CaO/Al_2O_3, Zr/Y, Ti/Zr) are not consistent with the basically chondritic values typical of Archaean komatiites (*e.g.*, Nesbitt & Sun, 1980). In the AFM diagram (Fig. 9a), these rocks define a high-Mg trajectory rather than a tholeiitic trend of magmatic differentiation expected for komatiites. Moreover, the high Mg values of most rocks (> 75) nearly rule out extensive crystal fractionation of komatitic melts. Instead, many of the geochemical features may easily be explained by strong olivine ± orthopyroxene accumulation in the course of igneous processes. The involvement of plagioclase into the fractionation/accumulaton process may not be concluded from our data. There is no prominent aluminum and lime enrichment and Eu reveals no essential anomaly in the normalized REE diagram, even for the most evolved low-Mg mafic rocks. However, Sr does show various anomalies in the ultramafic rocks, which might be attributed to either plagioclase fractionation or accumulation. However, Sr mobility during metamorphism must also be taken into consideration. Indeed, six out of eight samples which reveal a negative Sr anomaly are ultramafic amphibolites. It is noteworthy that in some of these rocks K also reveals strong positive anomalies probably due to potassium mobility during metamorphism. An overall LILE enrichment is prominent in most samples, which is confirmed by a light REE enrichment in the REE distribution patterns. Thus, we do not consider the Sr anomalies to indicate that plagioclase acted as a major petrogenetic factor. In consequence, we suggest that the rock forming magmatic processes did not take place at shallow crustal levels.

Samples sPCMMcue2, NRL 181, and NRL 180b form a subgroup of high-Si–Mg and low-Ca rocks which in part are only slightly metamorphosed and contain coarse orthopyroxene of likely cumulate origin. Their high silica, but low calcium contents may also be explained by an additional high-Si, low-Ca cumulate phase (amphibole?). Low HFSE abundances may also be readily explained by cumulate, rather than volcanic origin of these rocks.

In summary we suggest that the ultramafic to mafic blocks and lenses in the high-strain shear zones of the southern Mawson Escarpment represent tectonically dismembered and metamorphosed fragments of igneous rocks which mostly underwent strong chemical fractionation through cumulate processes at deeper crustal/upper mantle levels. In these rocks olivine was probably the most important cumulus

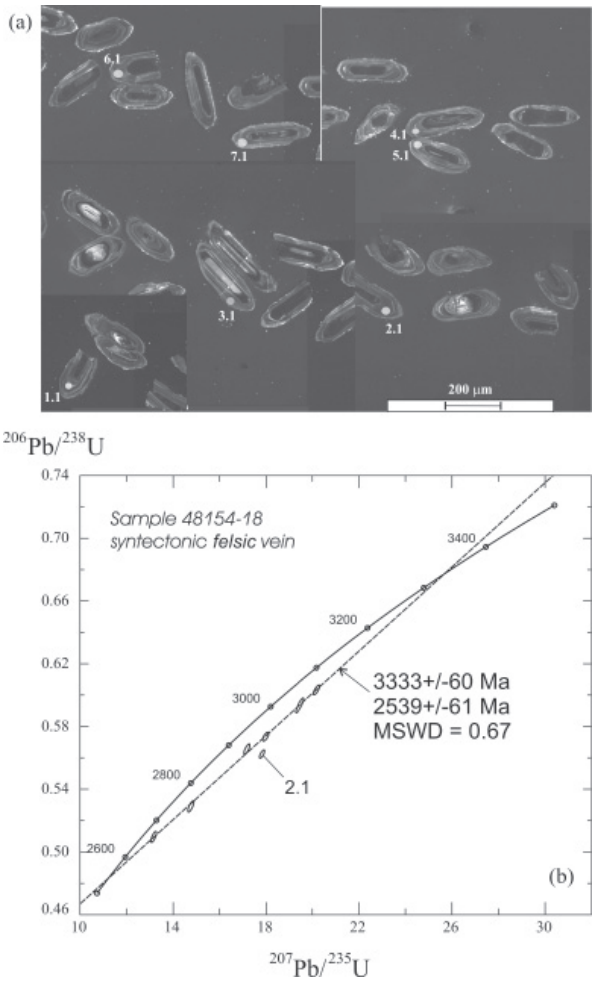

Fig. 8 - Cathodoluminescence images (a) and concordia plot for U-Pb SHRIMP analyses (b) of zircon from syntectonic felsic vein 48154-18 sampled from a high-strain shear zone at the NE Tingey Glacier. For discordia calculation, one outlier (2.1) has been omitted. Data points are shown with 1s errors while errors in intercept ages are calculated at 2σ level.

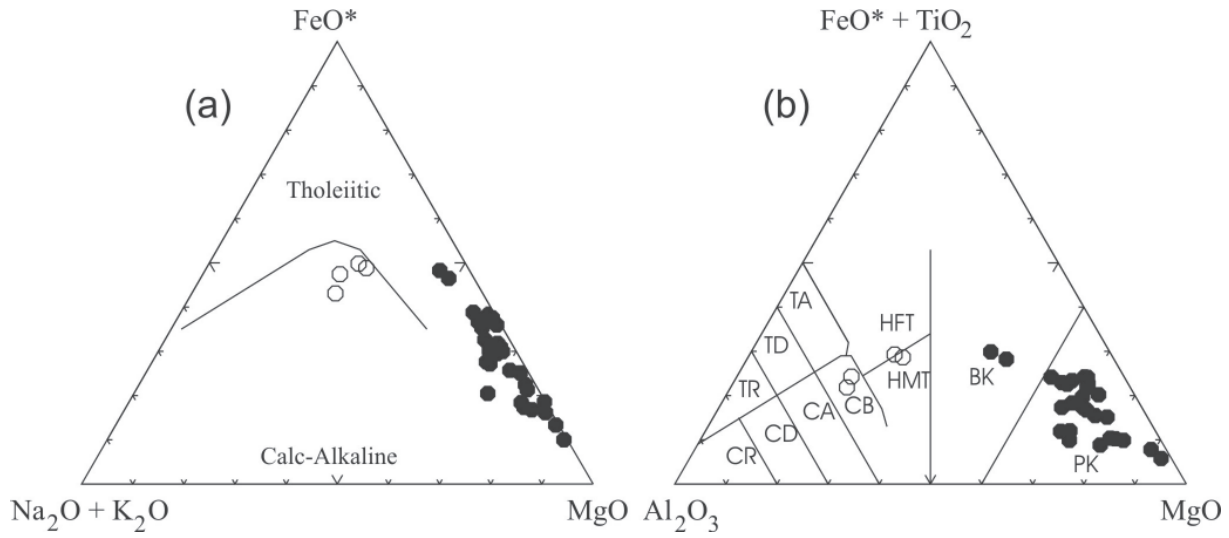

Fig. 9 - Ultramafic and mafic rocks from the southern Mawson Escarpment in a) AFM diagram after Irvine and Baragar (1971) and b) in the cation classification diagram after Jensen (1976). Abbreviations: PK, peridotitic komatiite; BK, basaltic komatiite; HFT, high-Fe tholeiite; HMT, high-Mg tholeiite; TA, tholeiitic andesite;CB, calc-alkaline basalt; TD, tholeiitic dacite;CA, calc-alkaline andesite;TR, tholeiitic rhyolite;CD, calc-alkaline dacite;CR, calc-alkaline rhyolite.

phase, while orthopyroxene and maybe also amphibole played a more subordinate role. However, for four samples with flat (sPCMTing3) or moderately light to middle REE enriched pattern (NRL 160, sPCM 64.2, sPCM 68.2), an origin from low-degree partial melts (NRL 160, sPCM 68.2: picritic basalts; sPCMTing3, sPCM 64.2: basalts) and thus a volcanic precursor can not be excluded. Very similar holds true for the mafic rocks sPCM62.5 and sPCM 69.4.

Sm-Nd ISOTOPE CONSIDERATIONS

The ultramafic and mafic rocks from the high-strain shear zones of the southern Mawson Escarpment have highly variable Sm/Nd ratios and the T_{DM} model ages. This is graphically shown in figure 10. Based on a two point (Cpx–WR) regression line for sample NRL 181, a slightly enriched isotopic composition with $\varepsilon_{Nd}(t = 3.9\ Ga) = -2$ can be inferred for the mantle source in the early Archaean. Enriched mantle sources have been previously reported for Neoarchaean basic metavolcanic and plutonic rocks from Mt. Ruker in the southern Prince Charles Mountains (Belyatsky et al., 2003). The isotope characteristics of these sources and the here obtained isotope composition for a mantle source in the southern Mawson Escarpment define an evolution trend in Fig. 10 which provides evidence that an enriched mantle source was present underneath the Ruker Terrane during the whole Archaean.

On the other hand, two ultramafic samples (sPCMMcue2, sPCMTing 2) have very high $f_{Sm/Nd}$ (0.17 and 0.35, respectively) and their T_{CHUR} model ages of ca 3.0 and 4.2 Ga, respectively, point to an origin from a highly depleted mantle source. The sample sPCMTing 2 closely matches the composition of the presumed early Archaean highly depleted mantle reported by Bennett et al. (1993) (Fig. 10). These two samples have only slightly fractionated (their primitive mantle-normalized values are close to unity) or spiked trace element distribution patterns in the spider diagram (Fig. 6), apart from the prominent enrichment in Sr, K, and Rb. The chondrite-normalized REE abundances in these two samples are also the most "primitive" with flat or slightly concave patterns. sPCMTing 2 shows a consistent depletion in the whole range of the REE, apart from Ce and La which display some probably secondary enrichment. Sample NRL 180b ($f_{Sm/Nd}$ = -0.32) which shows a heavy to middle REE depletion similar to sPCMTing 2 is however strongly enriched in the light REE. This is also evidenced by its Sm–Nd isotope data. Thus, sample NRL 180b probably represents an originally depleted rock similar to sPCMTing 2, which experienced a secondary enrichment in light REE and some other LILE (K, Rb, Pb). When an origin of NRL 180b from a material with Sm-Nd isotope characteristics of sPCMTing 2 is assumed, an age of *ca*. 3.6 Ga can be inferred for the secondary enrichment in incompatible elements in sPCMTing 2 from the age at which the Nd isotope evolution lines of both samples intersect (Fig. 10). At the present stage of study it is impossible to further constrain the age of the igneous precursors of the ultramafic to mafic rocks in the southern Prince Charles Mountains.

Sm-Nd isotope data for two gneisses (sPCM 62.8, sPCM 69.6) sampled from or close to shear zones are given for comparision. In their Sm-Nd isotope characteristics and model parameters, they closely compare to the orthogneisses from elsewhere in the Ruker Province (Mikhalsky et al. 2006b).

U-Pb AGE CONSIDERATIONS

The formation age of the ultramafic to mafic rocks is only weakly constrained. Sm–Nd isotope data suggest an early Archaean age of ca. 3.9 Ga for the protolith of sPCMTing 2. This is in accord with the U–Pb zircon age data for a syntectonic felsic vein

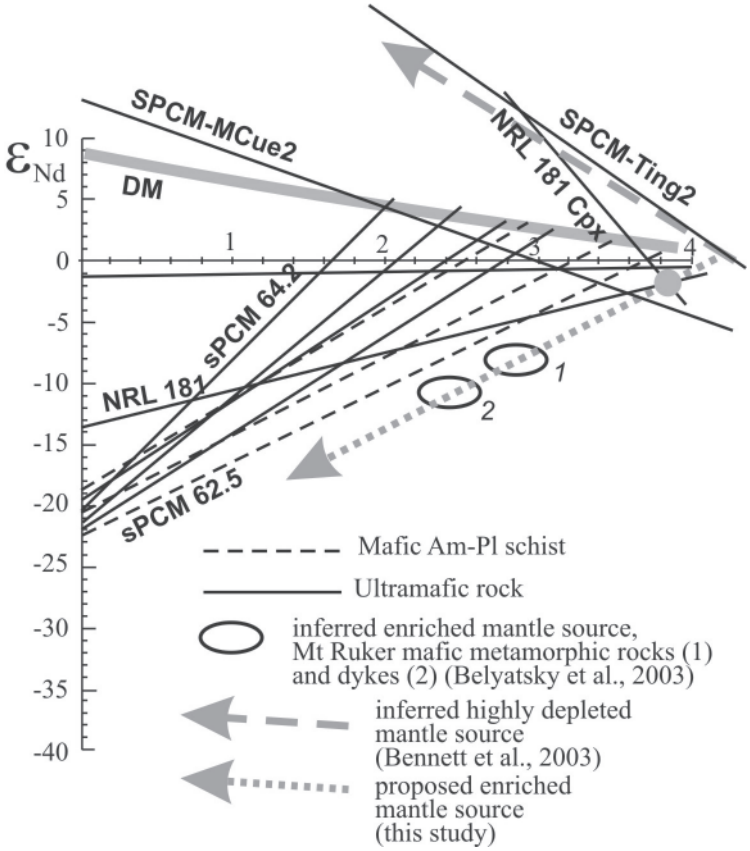

Fig. 10 - Sm–Nd isotope evolution of ultramafic and mafic rocks from high-strain shear zones of the southern Mawson Escarpment depicted in the ε_{Nd} vs age (in Ga) diagram. Calculated Nd isotope (in ε_{Nd} notation) evolution paths for ages of 0 – 4.5 Ga of samples are shown in black lines for ultramafics (solid lines) and mafics (dashed lines). Solid grey line indicates assumed Nd isotope evolution of depleted mantle (DM) from about 4 – 0 Ga. For details on other inferred isotope evolution paths and compositions for mantle sources (dashed grey lines and ellipses) see text.

(sample 48154-18) within the high-strain shear zone which can only provide a minimum age limit.

The upper and lower zircon intercept ages are interpreted to date crystallization/emplacement of the granitic vein within the shear zone at *ca.* 3333 ± 60 Ma and a subsequent (tectono-)thermal reworking event at *ca*. 2539 ± 61 Ma, respectively. The other alternative (upper intercept age indicative of zircon inheritance from a pre-existing source and lower intercept age representing the emplacement event) can be ruled out as the ages were obtained on oscillatory zoned areas of the crystals indicative for zircon crystallization in granitic melts. In that case, a discordant age pattern like that of zircons from sample 48154-18 is highly unlikely. Furthermore, we did not find evidence for a second magmatic growth event in the CL images of the zircons. Thus, the upper intercept age of *ca*. 3333 Ma most probably constrains the time of vein formation. In consequence, it also dates the formation of the high-strain shear zone including the entrainment of the ultramafic to mafic lenses and blocks. Within error, the upper intercept age of zircons 48154-18 matches the oldest so far reported magmatic U–Pb ages in this area. Similar ages were reported from felsic orthogneiss in McCue Bluff (zircon relict cores, 3370 ± 11 Ma, Boger et al., 2006) and from undeformed tonalite cobble enclosed in a diamictite of Neoproterozoic (Phillips et al., 2005) metasediments in Mt. Rubin (concordant zircon, 3392 ± 9 Ma, Mikhalsky et al., 2006b).

The lower intercept age of zircons 48154-18 of *ca*. 2539 Ma which is interpreted to date a (tectono-)thermal overprint is somewhat younger than the age of *ca*. 2645 Ma of an undeformed pegmatite vein (Boger et al., 2006) which crops out on the opposite (southern) side of the Tingey Glacier. So far, the c*a*. 2645 Ma date constrained a lower age limit for tectonothermal processes in the southern Mawson Escarpment. This indicates that latest Archaean (tectono-)thermal processes did not affected the metamorphic strata of the southern Mawson Escarpment (Ruker Province) pervasively. Interestingly, the lower intercept age of zircons 48154-18 fits within error to a *ca*. 2.5 Ga old major crustal formation episode which is well documented in the northerly adjoining Lambert Terrane (Mikhalsky et al., 2006b; Corvino & Henjes-Kunst 2007). One may thus speculate if localized (tectono-)thermal reworking in the Ruker Province was initiated by a major crust growth process in the Lambert Terrane.

CONCLUSIONS

The ultramafic and associated mafic rocks in high-strain shear zones of the southern Mawson Escarpment represent tectonically dismembered fragments of meta-igneous rocks which mostly formed through accumulation processes. In part, crystal fractionation processes may also have acted. The igneous protoliths of this suite of lithologically, geochemically and isotopically highly diverse rocks probably formed in the deeper crust/upper mantle in Eo- to Palaeoarchaean times. Relict clinopyroxene of one meta-igneous ultramafic rock yields a mineral-WR age of *ca*. 3.9 Ga ($\varepsilon_{Nd}(t)$ = -2) interpreted as the igneous crystallization age of this rock. The Sm–Nd isotope data point to the presence of either two different mantle sources in the southern Prince Charles Mountains, *i.e*. a highly depleted source and an enriched source, or a single highly depleted mantle source which experienced metasomatic enrichment (at c*a*. 3.6 Ga). The wide range of trace element and Sm-Nd isotope compositions of this rock suite suggests

that a metasomatic enrichment of a depleted mantle source is a more appropriate option.

The tectonic emplacement of these rocks in high-strain shear zones within orthogneiss of the Ruker Province occurred in Paleoarchaean times (*ca*. 3.3 Ga) in a compressive regime and closely follows in time a major crustal growth episode of the Ruker Province (formation of igneous precursor of the orthogneiss at *ca*. 3.4 Ga). The high-strain shear zones are interpreted as deep reaching major crustal shear zones which tectonically incorporated compositional highly divers fragments from the deeper crust/upper mantle. They compare well to, for instance, prominent tectonic melange zones in the Central European Alps ("TAC" of Berger et al. 2005) and may thus be interpreted as "melange zones" typical for major crustal suture zones formed at different stages during continental collisional geotectonic processes (Brouwer et al. 2005). Within the Ruker Province of the southern Mawson Escarpment, however, we have presently no evidence for different continental blocks on both sides of the melange zones. Nevertheless, we assume that the melange zones are indicators of a compressive tectonic regime related to the collision of continental blocks to form the tectonic grid of the Ruker Province in the Paleo- to Mesoarchaean.

Acknowledgements - The Australian Antarctic Division personnel provided friendly and professional logistic and field support during the PCMEGA 2002/2003. Some analysed samples were earlier collected by E.N. Kamenev, V.M. Mikhailov, L.V. Fedorov whose field data are acknowledged. S.A. Sergeev is thanked for carrying out the SHRIMP analyses at the Isotopic Center (VSEGEI, St Petersburg). This study was supported by the Russian governmental Federal Programme "World Ocean", subprogram "Antarctica". This work was made possible in part by a grant from Deutsche Forschungsgemeinschaft (DFG) and the Russian Foundation for Basic Research grant 07–05–01001 to EVM. Don Henry, Peter Rendschmidt, Julian Lodziak, Frank Melcher, Detlef Requard, Frank Korte, Monika Bockrath, Siegrid Gerlach and Peter Macaj are thanked for laboratory assistance at the BGR, Hannover. Critical reviews by Franco Talarico, Uli Schüssler and Chris Wilson helped to improve the manuscript.

REFERENCES

Belyatsky B.V., Kamenev E.N., Laiba A.A. & Mikhalsky E.V., 2003. Sm–Nd ages of metamorphosed volcanic and plutonic rocks from Mount Ruker, the southern Prince Charles Mountains, East Antarctica. Programme and Abstracts, *9th International Symposium on Antarctic Earth Sciences. Schriften der Alfred-Wegener-Stiftung* 2003/2004, 24–25.

Bennett V.C., Nutman A.P. & McCulloch M.T., 1993. Nd isotopic evidence for transient, highly depleted mantle reservoirs in the early history of the Earth. *Earth and Planetary Science Letters*, **119**, 299-317.

Berger A., Mercolli I. & Engi M., 2005. The central Lepontine Alps: Notes accompanying the tectonic and petrograpgic map sheet Sopra Ceneri (1:100'000). *Schweizer Mineralogische und Petrographische Mitteilungen*, **85**, 109-146.

Black, L.P. & Kamo, S.L., 2003. TEMORA 1: a new zircon standard for U-Pb geochronology. *Chemical Geology*, **200**, 155-170.

Boger S.D., Wilson C.J.L. & Fanning C.M., 2001. Early Paleozoic tectonism within the East Antarctic Craton: the final suture between east and west Gondwana? *Geology*, **29**, 463-466.

Boger S.D., Wilson C.J.L. & Fanning C.M., 2006. An Archaean province in the southern Prince Charles Mountains, East Antarctica: U–Pb zircon evidence for c. 3170 Ma granite plutonism and c. 2780 Ma partial melting and orogenesis. P*recambrian Research*, **145**, 207–228.

Brouwer F.M., Burri T., Engi M. & Berger A., 2005. Eclogite relics in the Central Alps: PT-evolution, Lu-Hf ages and implications for formation of tectonic melange zones. *Schweizer Mineralogische und Petrographische Mitteilungen*, **85**, 147-174.

Cerrai E. & Testa C., 1963. Separation of rare earths by means of small columns of Kel-F supporting di(2-ethylhexyl)ortop hosphoric acid. *Journal Inorganic Nuclear Chemistry*, **25**, 1045-1050.

Corvino A.F. & Henjes-Kunst F., 2007. A record of 2.5 and 1.1 billion year old crust in the Lawrence Hills, Antarctic Southern Prince Charles Mountains. *Terra Antartica,* **14**(1), 13-30.

DePaolo, D.J., 1988. *Neodymium Isotope Geochemistry. An Introduction*. Springer Verlag Berlin Heidelberg New York London Paris Tokyo, 187 p.

Irvine T.N. & Barager W.R.A., 1971. A guide to the chemical classification of the common volcanic rocks. *Canadian Journal of Earth Sciences*, 8, 523-548.

Jacobsen, S.B. & Wasserburg, G.J., 1980. Sm-Nd isotopic evolution of chondrites. *Earth and Planetary Science Letters*, **50**, 139-155.

Jensen L.S., 1976. A New Cation Plot for Classifying Subalkalic Volcanic Rocks. *Ontario Division of Mines*, **MP 66**, 22 p.

Kretz R., 1983. Symbols for rock-forming minerals. *American Mineralogist*, **68**, 277–279.

Kamenev E.N., 1993. Structure and evolution of the Antarctic shield in Precambrian. In: Findley R.H., Unrug R., Banks M.R. & Veevers J.J. (eds.), Gondwana eight: assembly, evolution and dispersal. Balkema, Rotterdam, 141–151.

Kamenev E.N., Kameneva G.I., Mikhalsky E.V. & Andronikov A.V., 1990. The Prince Charles Mountains and Mawson Escarpment (in Russian). In: Ivanov V.L. & Kamenev E.N. (eds.), *The geology and mineral resources of Antarctica* (in Russian). Nedra, Moscow, 67–113.

Le Maitre R.W., Bateman P., Dudek A., Keller J., Lameyre J. Le Bas M.J., Sabine P.A. Schmid R., Sorensen H., Streckeisen A., Woolley A.R. & Zanettin B., 1989. *A Classification of Igneous Rocks and Glossary of terms: Recommendations of the International Union of Geological Sciences Subcommission on the Systematics of Igneous Rocks*. Blackwell Scientific Publications, Oxford, U.K.

Ludwig K.R., 1999. User 's manual for Isoplot/Ex, Version 2.10, A geochronological toolkit for Microsoft Excel. *Berkeley Geochronology Center Special Publication* No. **1a**, 2455 Ridge Road, Berkeley CA 94709, USA.

Ludwig K.R., 2000. SQUID 1.00, A User's Manual; *Berkeley Geochronology Center Special Publication*. No. **2**, 2455 Ridge Road, Berkeley, CA 94709, USA.

Mikhalsky E.V., Sheraton J.W., Laiba A.A., Tingey R.J., Thost D.E., Kamenev E.N. & Fedorov L.V., 2001. Geology of the Prince Charles Mountains, Antarctica. *AGSO - Geoscience Australia Bulletin* **247**, 209 p.

Mikhalsky E.V., Laiba A.A., Beliatsky B.V., 2006a. The composition of the Prince Charles Mountains: a review of geologic and isotopic data. In: Futterer D. et al. (eds.), *Antarctica: Contributions to global earth sciences*. Springer-Verlag, Berlin Heidelberg New York, 69-82.

Mikhalsky E.V., Beliatsky B.V., Sheraton J.W., Roland N.W., 2006b. Two distinct Precambrian terranes in the southern Prince Charles Mountains, East Antarctica: SHRIMP dating and geochemical constraints. *Gondwana Research*, **9**, 291-309.

Mikhalsky E.V., Henjes-Kunst F. & Roland N.W., 2007. Early Precambrian mantle derived rocks in the southern Prince Charles Mountains, East Antarctica: age and isotopic constraints. In: Cooper A.K. & Raymond C.R. (eds.): *Antarctica: A Keystone in a Changing World* - online Proceedings of the 10th ISAES, USGS Open-File Report 2007-1047, Short Research Paper 039, 4 p.; DOI:10.3133/of2007-1047.srp039

Nesbitt R.W. & Sun S.-S., 1980. Geochemical features of some Archaean and post-Archaean high-magnesian–low-alkali liquids. *Phil. Transactions Royal Society London*, **A297**, 365–381.

Phillips G., Wilson C.J.L. & Fitzsimons I.C.W., 2005. Stratigraphy and structure of the southern Prince Charles Mountains, East Antarctica. *Terra Antartica*, **12**, 69–86.

Phillips G., Wilson C.J.L., Campbell I.H. & Allen C.M., 2006. U–Th–Pb detrital zircon geochronology from the southern Prince Charles Mountains, East Antarctica – defining the Archaean to Neoproterozoic Ruker Province. *Precambrian Research*, **148**, 292–306.

Sun S.-S. & McDonough W.F., 1989. Chemical and isotopic systematics of oceanic basalts: implications for mantle composition and processes. In: Saunders A.D. & Norry M.J. (eds.), Magmatism in the ocean basins. *Geological Society Special Publication* **42**, 313–345.

Tingey R.J., 1991. The regional geology of Archaean and Proterozoic rocks in Antarctica. In: Tingey RJ (ed.), *The geology of Antarctica*. Clarendon Press, Oxford, 1–58.

Wetherill G.W., 1956. Discordant uranium-lead ages. *Transactions American Geophysical Union*, **37**, 320-326.

Williams I.S., 1998. U-Th-Pb Geochronology by Ion Microprobe. In: McKibben, M.A., Shanks III, W.C. and Ridley, W.I. (eds), Applications of microanalytical techniques to understanding mineralizing processes. *Reviews in Economic Geology*, **7**, 1–35.